Supporting Information

Defect-Induced Subgap State Engineering in Neuromorphic Metal-Oxide Phototransistors for In-Sensor Color Processing

Eun Chong Ju[1], Dong Hwan Byeon[1], Jong Min Lee[1], Yu-Jung Cha[2,6], Hyung Gon Shin[3], Seongil Im[3], Jeong-Wan Jo[4], Yong-Hoon Kim[5]*, Sung Kyu Park[1]*, Sung Woon Cho[2]*

[1] Department of Intelligent Semiconductor Engineering, Chung-Ang University, Seoul, 06974 Republic of Korea

[2] Department of Advanced Components and Materials Engineering, Sunchon National University, Suncheon, Jeonnam 57922, Republic of Korea

[3] Department of Physics and Applied Physics, Yonsei University, Seoul 03722, Republic of Korea

[4] Electrical Engineering Division, Department of Engineering, University of Cambridge, 9 JJ Thomson Avenue, Cambridge CB3 0FA, UK

[5] School of Advanced Materials Science and Engineering, Sungkyunkwan University, Suwon 16419, Republic of Korea

[6] Department of Energy Technology, Korea Institute of Energy Technology, Naju, Jeonnam 58330, Republic of Korea

* Correspondence and requests for materials should be addressed to S. K. Park (skpark@cau.ac.kr), S. W. Cho (swcho@scnu.ac.kr) and Y. H. Kim (yhkim76@skku.edu).

This "Supporting Information" includes:

Figure S1 to S16

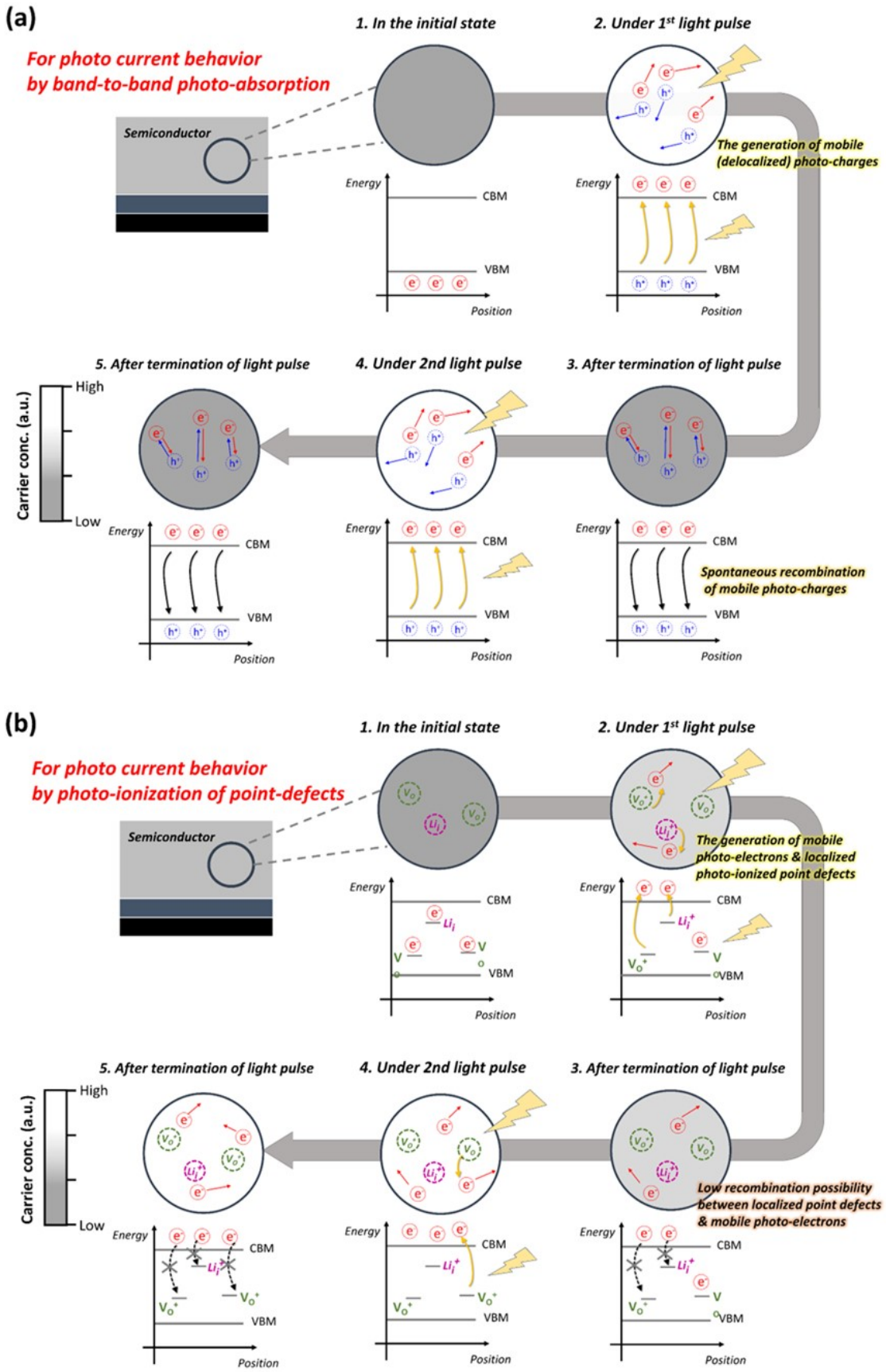

fig. S1. Schematic showing recombination process of photocharges formed in a semiconductor film under repeated light irradiation: (a) band-to-band recombination between delocalized photocharges, (b) recombination between delocalized photo-electrons and localized ionized point defects.

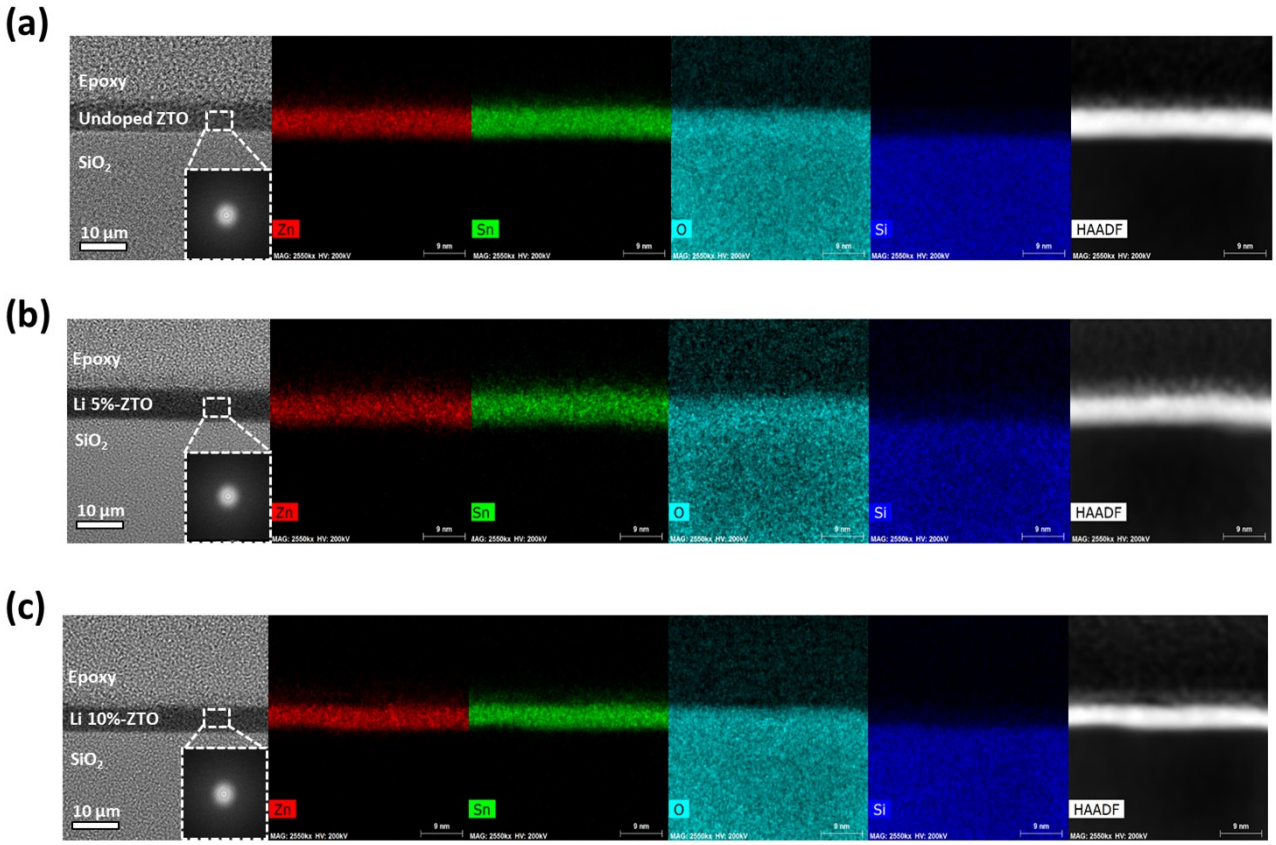

fig. S2. Cross-sectional transmission electron microscope images and energy dispersive X-ray spectroscopy mapping data of ZTO-based films: (a) undoped ZTO, (b) Li (5 at %)-ZTO, and (c) Li (10 at %)-ZTO.

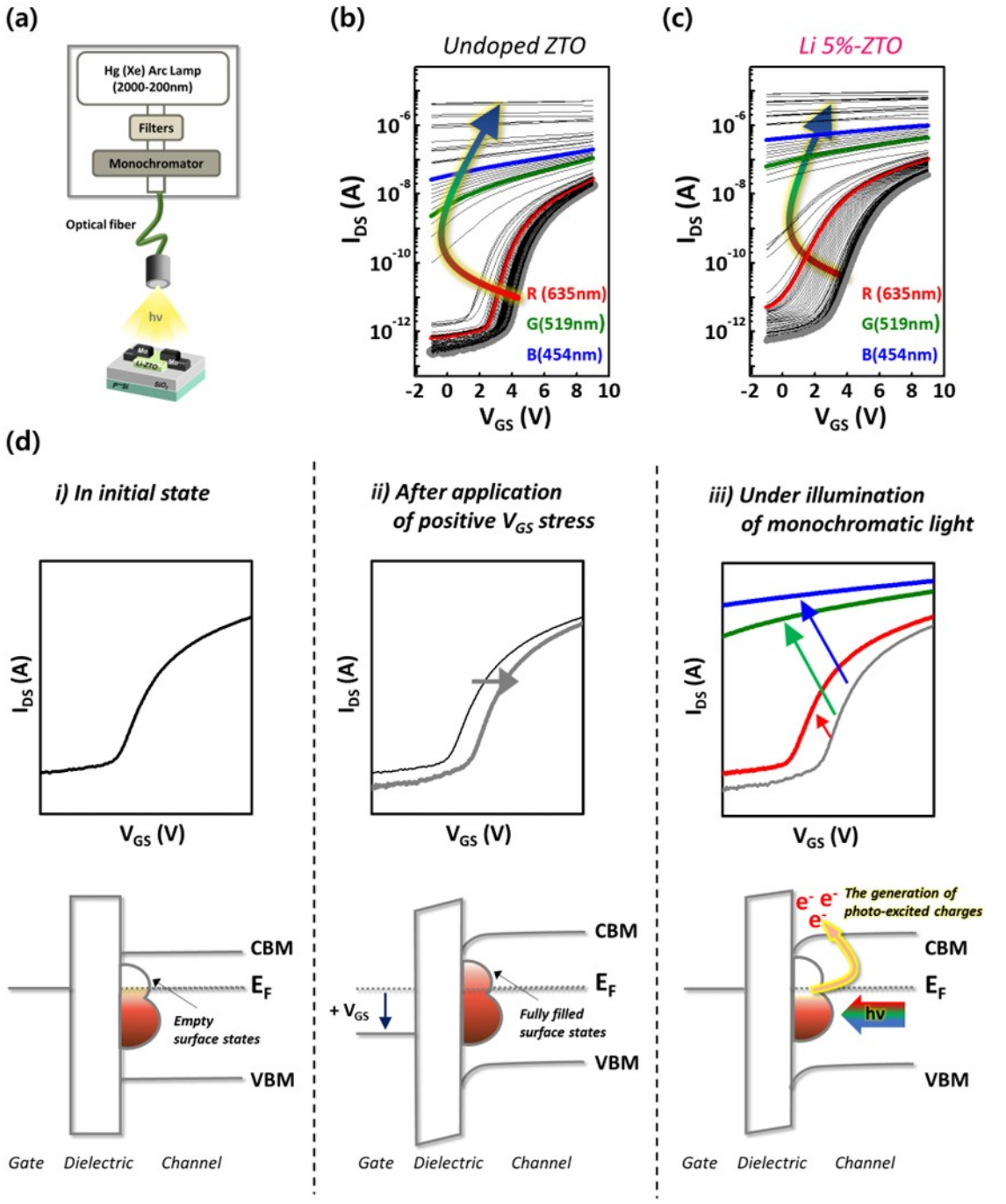

fig. S3. (a) Photo-excited charge collection spectroscopy (PECCS) measurement setup: a Hg (Xe) arc lamp (200–2000 nm), an optical filter with a diameter of 200 μm for NIR-VIS-UV light, and a grating monochromator. The monochromatic lights of various wavelengths were used at identical power of 0.1 mW/cm². (b, c) PECCS measurement results for the samples: (b) undoped ZTO and (c) Li (5 at %)-ZTO device. (d) Band diagram schematics and transfer curves of the sample, depending on the measurement steps for PECCS analysis.

PECCS measurements to estimate the subgap density of states (DOS) of the semiconductor channel were performed using the instrument setup shown in Fig. S2a. Figs. S2b and S2c show the transfer curves of undoped ZTO and Li (5 at %)-ZTO devices acquired by PECCS measurement, respectively. As shown in Fig.

S2d, before illumination of monochromic light, the empty subgap states of the semiconductor channel located at the channel/dielectric interface are filled with electrons by V_{GS} sweeping. Here, as the subgap DOS is gradually filled with electrons, the transfer curve shifts toward the positive direction. Next, samples are irradiated with monochromatic light after ensuring that the positive change in the transfer curve has reached saturation. When monochromatic light is sequentially irradiated from low energy to high energy, the trapped charges begin to be released stepwise from shallower subgap states. These photo-released charges cause a shift in the negative direction of the transfer curve and a change of the threshold voltage (V_{Th}). Next, by estimating flatband voltage (V_{FB}) from transfer curves acquired under monochromatic lights with various photon energies, the subgap DOS can be calculated from the change in flat-band voltage as a function of photon energy using the following equation:

$$D_{it}(CBM - e) = \frac{C_{0x}\partial V_{FB}}{q \quad \partial_e}$$

, where D_{it}, Cox, q, and $\partial V_{FB}/\partial e$ represent the subgap DOS, the capacitance of oxide gate dielectric, electronic charge, and the variation in V_{FB} as a function of photon energy, respectively.

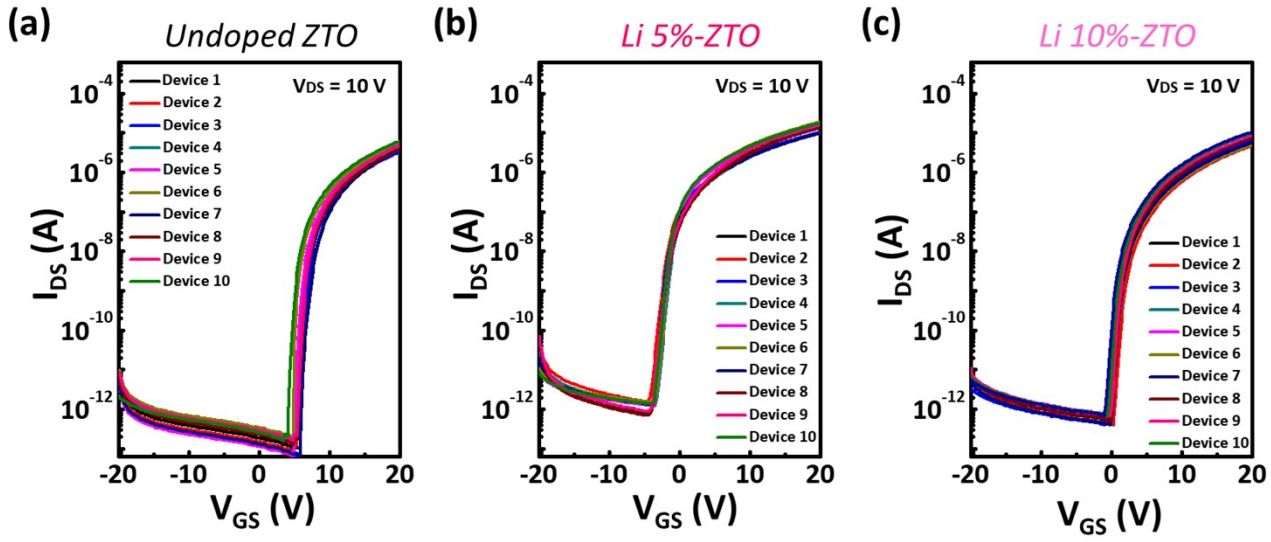

fig. S4. Transfer curves of 10 ZTO-based phototransistors: (a) undoped ZTO, (b) Li (5 at %)-ZTO, and (c) Li (10 at %)-ZTO.

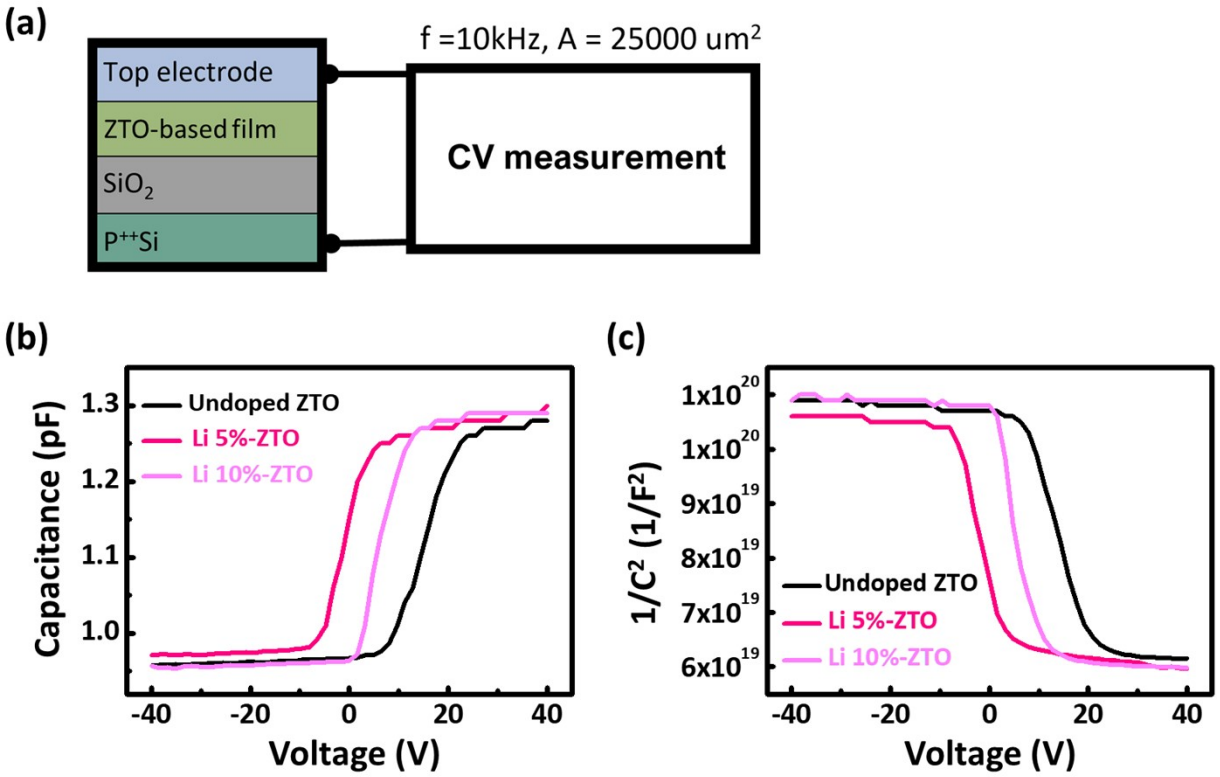

fig. S5. (a) A schematic diagram for capacitance-voltage (C-V) measurement. (b) C-V and (c) $1/C^2$-V curves measured from metal-insulator-semiconductor (MIS; p^{++}-Si/SiO_2/ZTO-based films) structures.

As shown in Figure S4, the C-V and $1/C^2$-V curves of the MIS samples including the ZTO-based films are measured to estimate the carrier concentration of the ZTO-based films. Based on Figure S4b, the carrier concentration (n) of ZTO-based films can be estimated by the following equation:

$$n = -2\left[q\varepsilon_s\left(\frac{dC^{-2}}{dV}\right)\right]_{-1}$$

, where q is the electron charge, and ε is the permittivity of the ZTO-based film with varying Li content. The carrier concentrations of undoped ZTO, Li (5 at %)-ZTO, and Li (10 at %)-ZTO estimated through C-V measurement were 8.74×10^{17} cm^{-3}, 8.23×10^{18} cm^{-3}, and 4.88×10^{18} cm^{-3}, respectively.

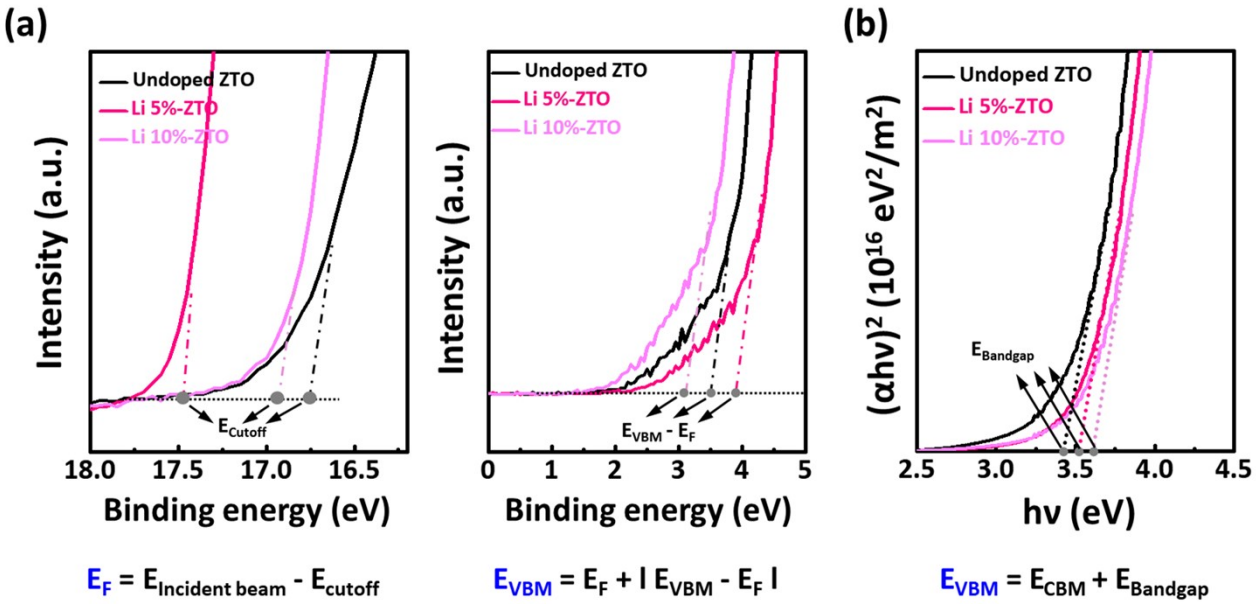

fig. S6. (a) A UPS spectrum and (b) a Tauc plot of the ZTO-based films, indicating energies of the secondary electron cut-off and valence band onset and energy band gap, respectively.

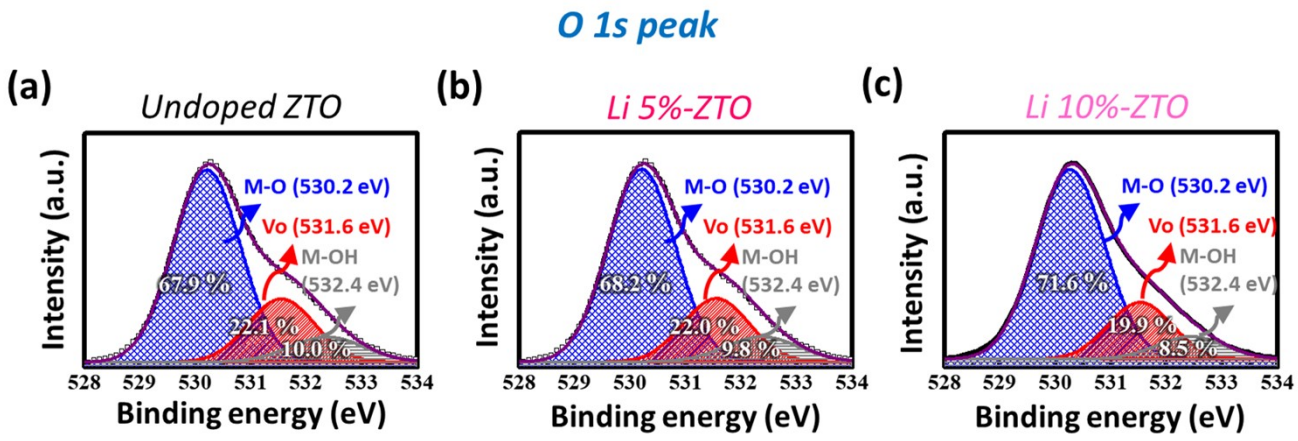

fig. S7. XPS O 1s spectra of ZTO-based films: (a) undoped ZTO, (b) Li (5 at %)-ZTO, and (c) Li (10 at %)-ZTO.

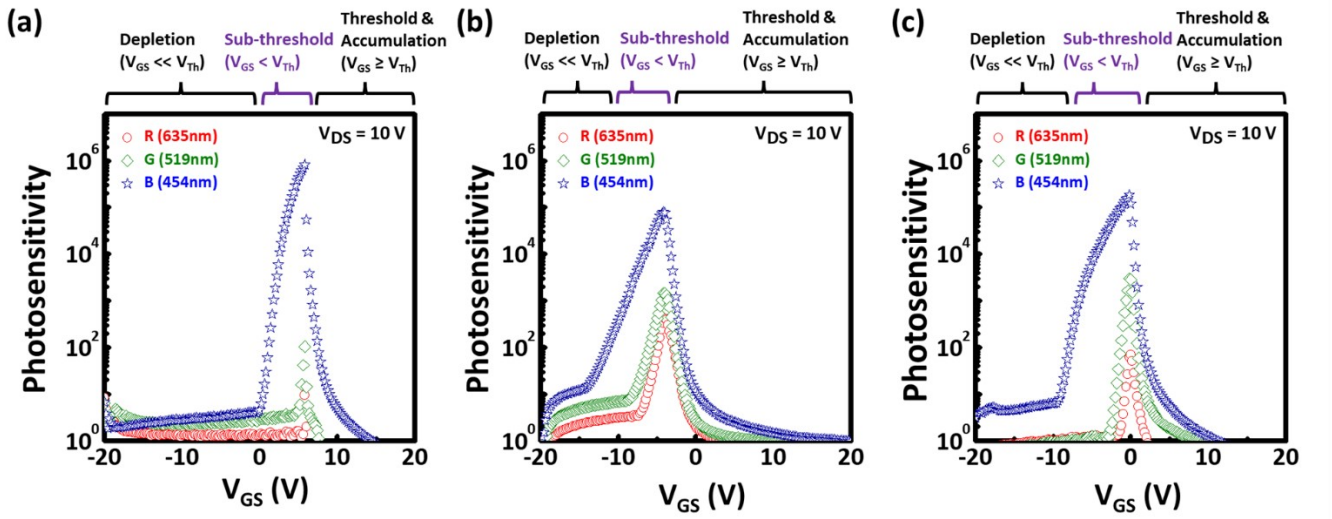

fig. S8. Photosensitivity of ZTO-based phototransistors under R/G/B light illumination at various gate voltage conditions: (a) undoped ZTO, (b) Li (5 at %)-ZTO, and (c) Li (10 at %)-ZTO. Photosensitivity, which is calculated by the relative change in current under light exposure, was estimated using the following equation: Photosensitivity = $(I_{Photo}-I_O) / I_O$, I_{Photo}, I_O represent the photocurrent of phototransistor under light illumination, the original current of phototransistor under dark state. The power density of each R, G, and B lights is 7 mW cm^{-2}.

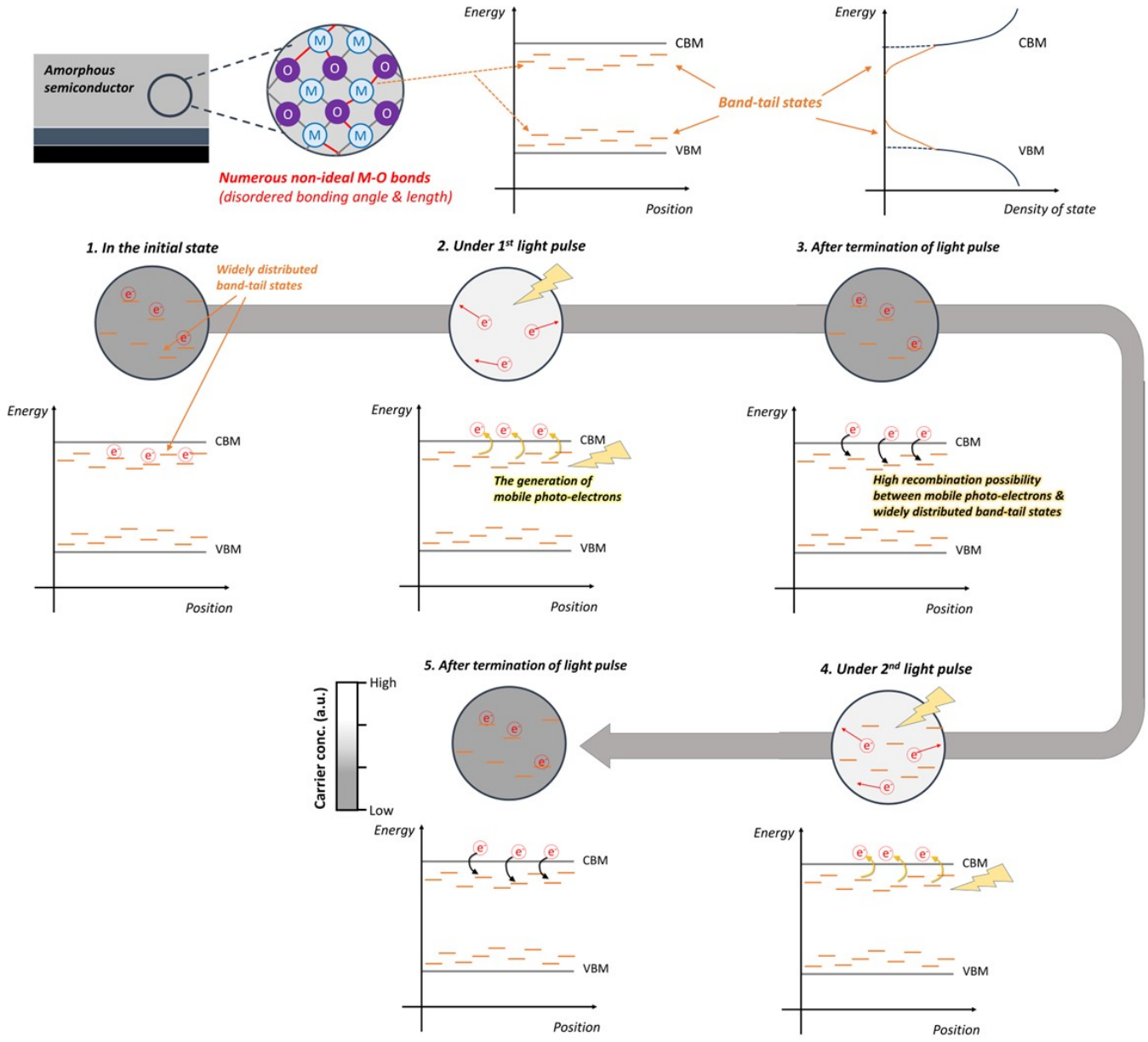

fig. S9. Schematic illustrating the recombination process between delocalized photoelectrons and widely distributed band-tail states in an amorphous oxide semiconductor.

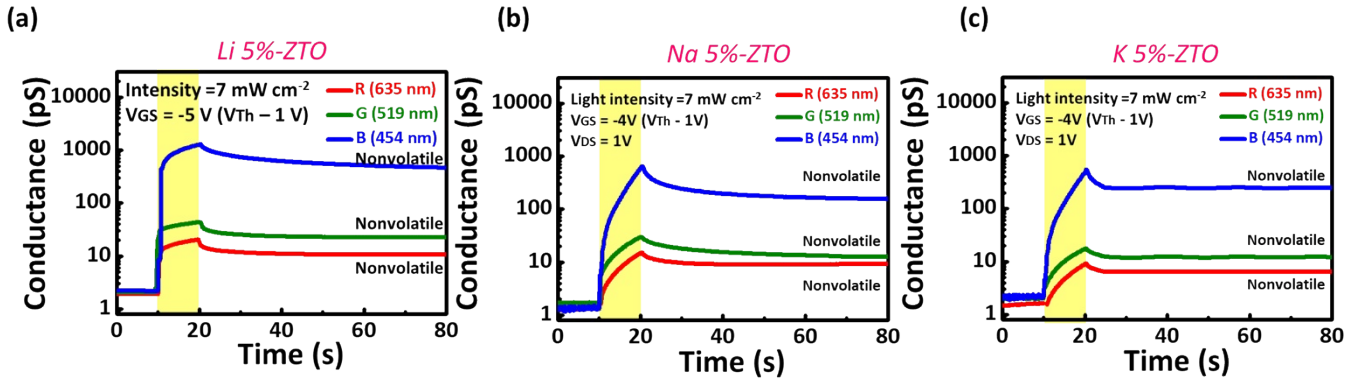

fig. S10. Nonvolatile memory characteristics of alkali metal-doped ZTO phototransistors under RGB illumination. (a) 5% Li-doped ZTO, (b) 5% Na-doped ZTO, and (c) 5% K-doped ZTO.

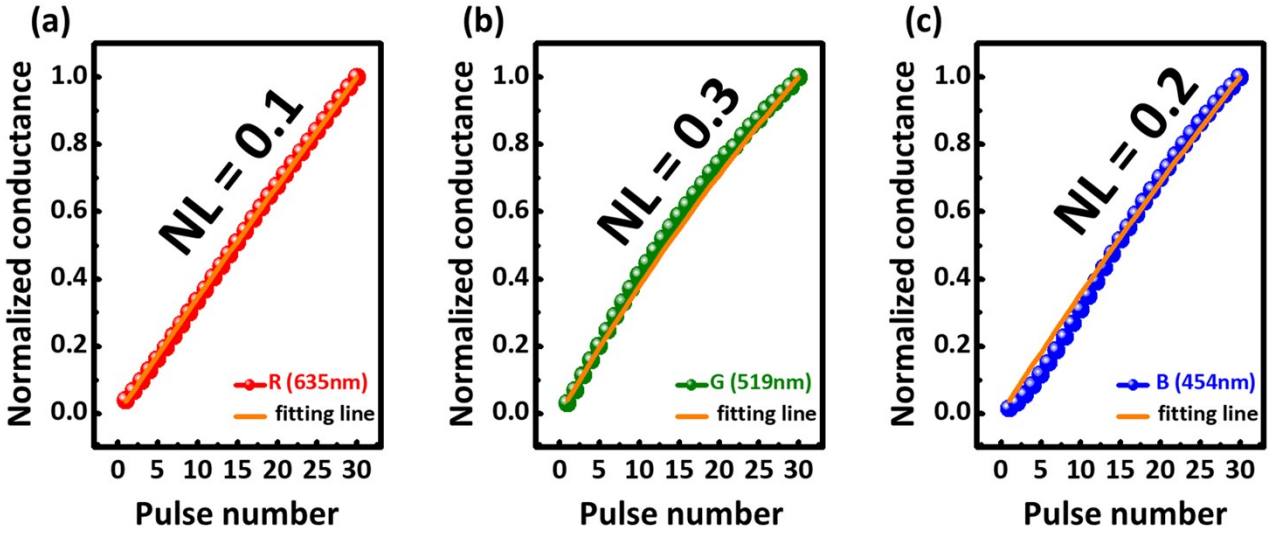

fig. S11. Normalized conductance of Li (5 at %)-ZTO phototransistors. Nonlinearity (NL) values of Li (5 at %)-ZTO device under R, G, and B light pulses are 0.1, 0.3, and 0.2, respectively.

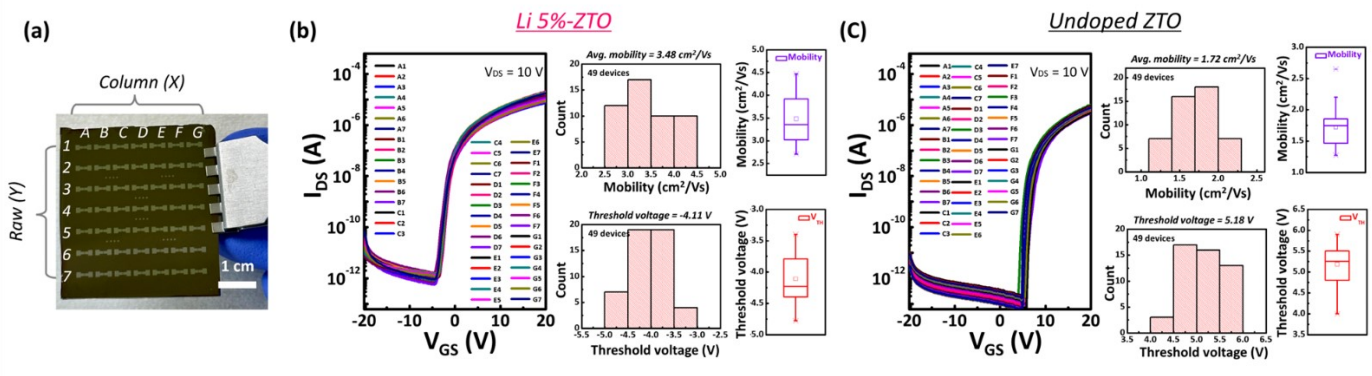

fig. S12. (a) Device position on 7×7 phototransistor array. (b, c) Transfer curve and performance uniformity (mobility and threshold voltage) of 49 devices on a phototransistor array: (b) Li (5 at %)-ZTO and (c) undoped ZTO device

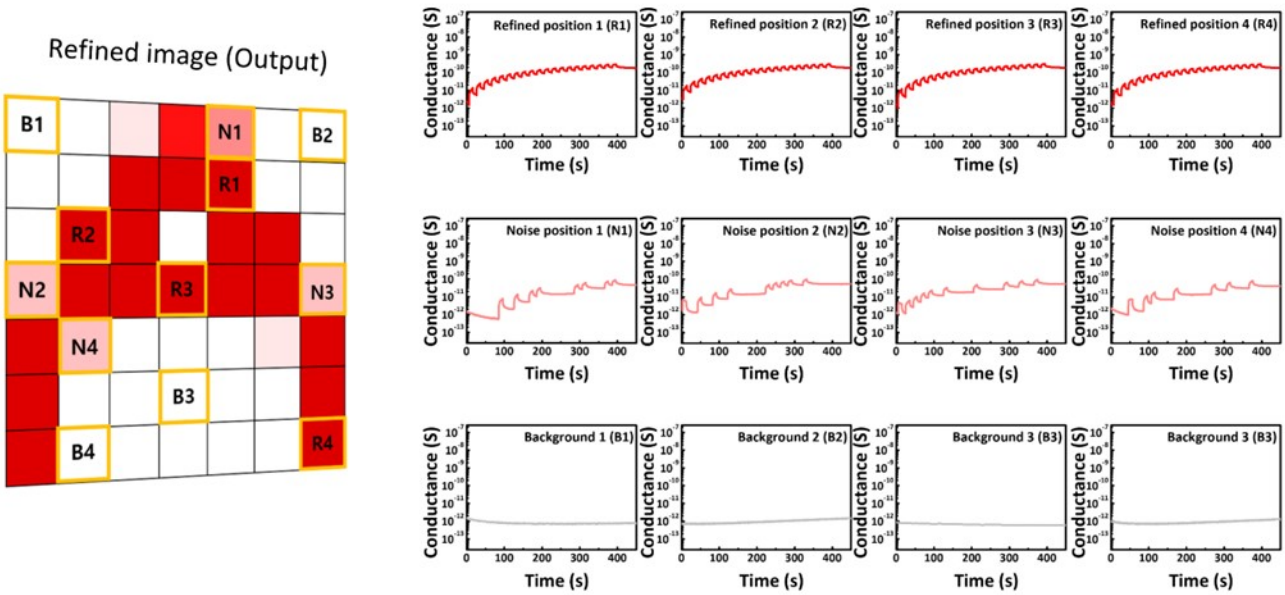

fig. S13. Actual neuromorphic conductance updating results of Li (5 at %)-ZTO phototransistors present in each pixel of neuromorphic vision sensor under 'A' pattern input of red color.

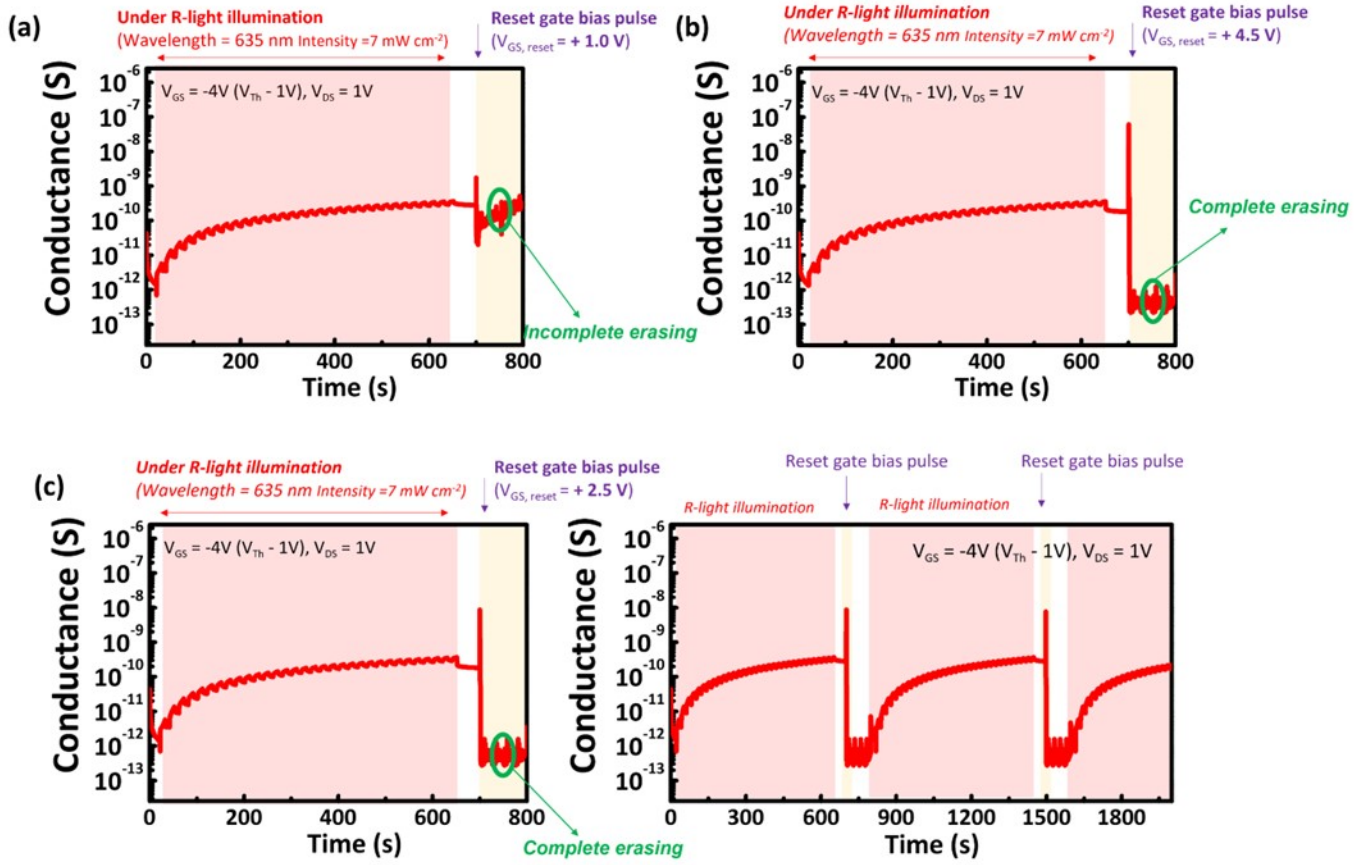

fig. S14. The erasing behavior results of the conductance states in Li(5 at %)-ZTO phototransistors by various reset gate bia pulse ($V_{GS,\ reset}$) conditions: (a) $V_{GS,\ reset}$ = + 1.0 V, (b) + 4.5 V and (c) + 2.5V for 2 s.

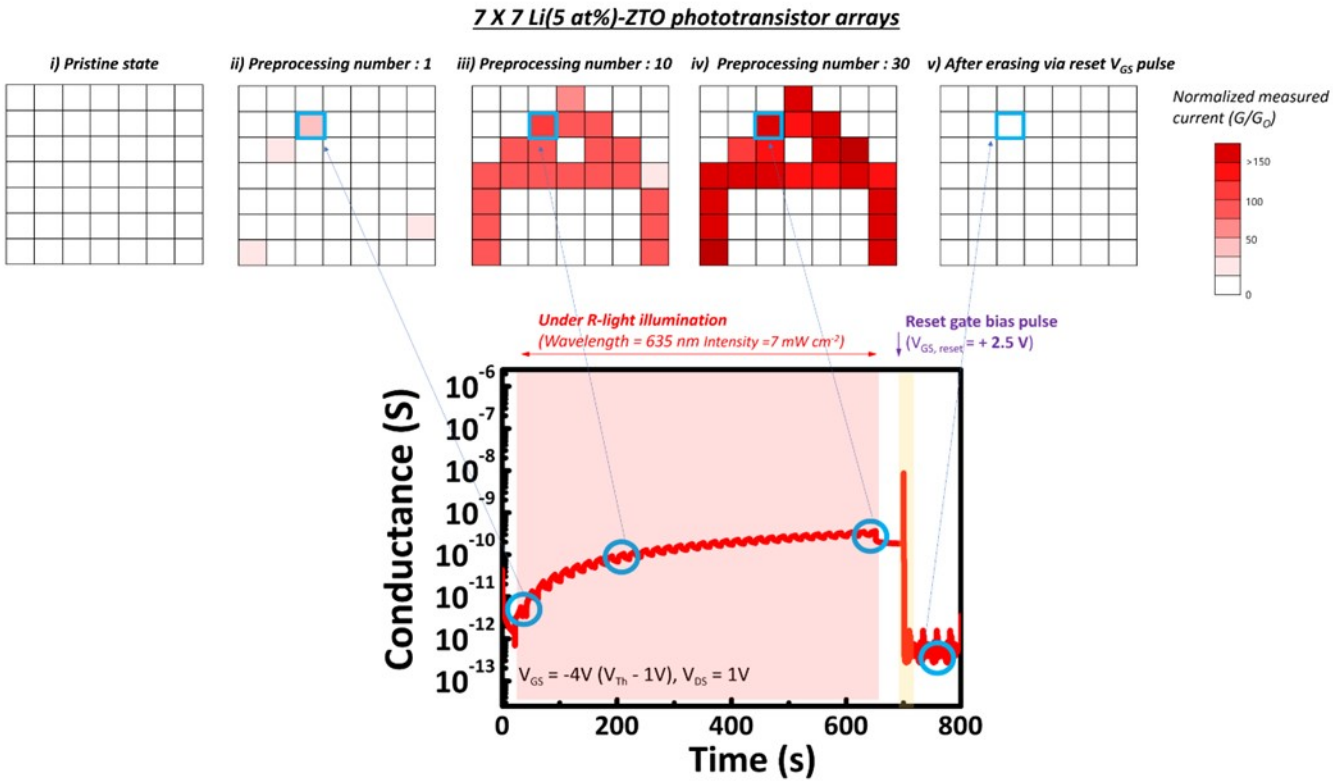

fig. S15. Conductance updating behavior of Li (5 at %)–ZTO phototransistor arrays under repeated inputs of red letter 'A' images (i.e., increased number of preprocessing operations), and their complete reset operation by applying a gate bias pulse ($V_{GS, reset}$ = + 2.5 V).

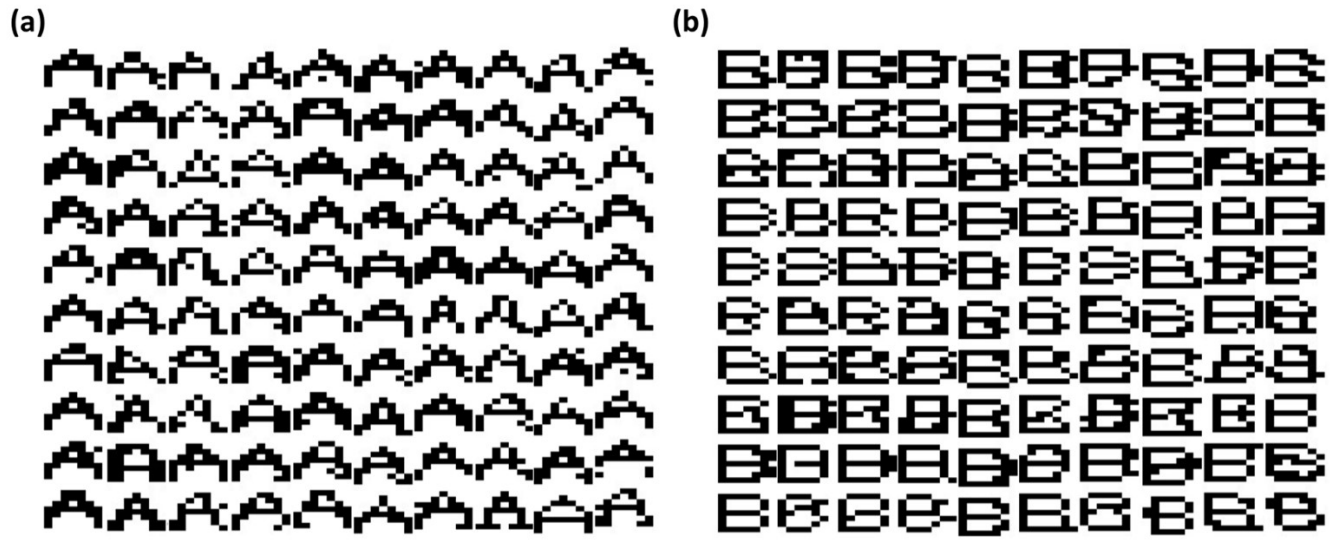

fig. S16. Raw data set for (a) 'A' and (b) 'B' patterns (100 images of different shapes).

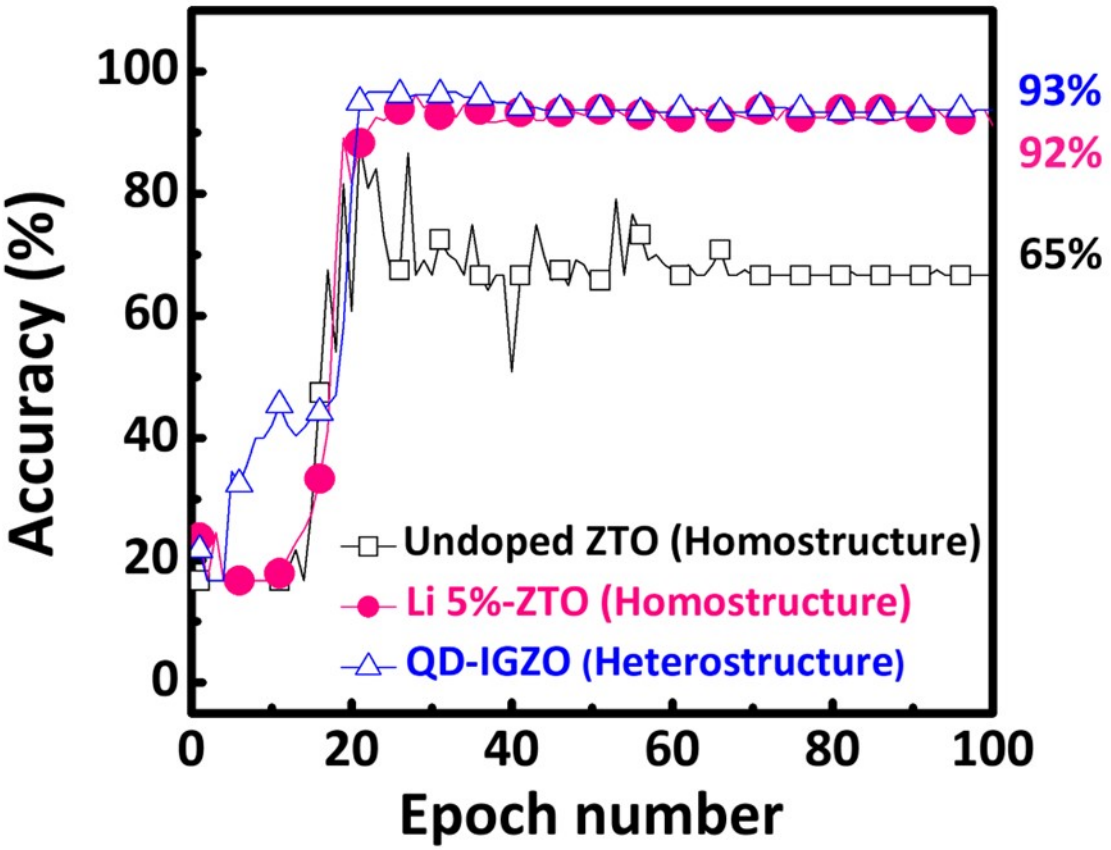

fig. S17. Performance comparison of pattern recognition tasks using neuromorphic image processors with homostructure and heterostructure channel architecture. The case using the heterostructure quantum dot (QD)-InGaZnO (IGZO) channel achieved a pattern recognition accuracy of 93 % after 100 training epochs.

Table S1. Comparison of representative in-sensor image-processing characteristics of neuromorphic MO phototransistors with homostructure and heterostructure channel configurations.

Channel		RGB response	Conductance	Pulse number	Application	REF
Structure	Material					
Heterostructure	M QD/IGZO	R	1.1E-9	30	Monochromatic (R, G, B) & mixed color image processing	[S1]
		G	6.5E-7			
		B	8E-5			
	IGZO/TE/QD	R	5.5E-7	10	Monochromatic (R, G, B) color image processing	[S2]
		G	1.8E-7			
		B	8.5E-8			
Homostructure	Cd doped IGZO	G	3.0E-9	30	Monochromatic (G, B) & mixed color image processing	[S3]
		B	1.3E-7			
	N doped ZnSnO	R	N.A.	20	Monochromatic (B) color image processing	[S4]
		G	N.A.			
		B	1.1E-8			
	Undoped ZnSnO	R	3.6E-12	30	Monochromatic (R, G, B) & mixed color image processing	**This study**
		G	5.1E-12			
		B	2.0E-10			
	Li doped ZnSnO	R	3.6E-10	30		
		G	2.4E-9			
		B	1.0E-7			

[S1] C. Jo, J. Kim, J. Y. Kwak, S. M. Kwon, J. B. Park, J. Kim, G. S. Park, M. G. Kim, Y. H. Kim and S. K. Park, *Adv. Mater.*, 2022, **34**, 2108979.

[S2] R. Dutta, M. Naqi, Y. Cho, J. Oh, T. Kim, U. Jeong, Y. Yu, Y. Lee, S. Kim, *Adv. Funct. Mater.*, 2024, **34**, 2315058.

[S3] J. H. Jeong, M. H. Park, H. Jeong, W. Kim, S. Park, W. Jeon, S. J. Kang, *ACS Appl. Electron. Mater*., 2023, **5**, 6275−6285.

[S4] X. Liu, J. Ren, P. Hu, Y. Qian, T. Li, L. Liang, H. Cao, *Phys. Status Solidi RRL*, 2024, **18**, 2300490.

Table S2. Comparison of the representative optoelectronic performance of neuromorphic MO phototransistors with homostructure and heterostructure channel configurations.

Channel		Photoresponse					Power Consumption	REF
Structure	Material	Wavelength (nm)	Conductance switching	I_{photo} (A)	V_{read} (V)	Time (s)		
Heterostructure	M QD/IGZO	635 (R)	Non-volatile	2.5E-12	1	0.2	0.50 pJ	[S1]
		519 (G)	Non-volatile	3.92E-10			78.33 pJ	
		405 (B)	Non-volatile	6.52E-8			13.03 nJ	
	IGZO/TE/QD	680 (R)	Non-volatile	4.5E-8	1	5	225 nJ	[S2]
		532 (G)	Non-volatile	1.1E-7			550 nJ	
		405 (B)	Non-volatile	5.0E-7			2500 nJ	
Homostructure	Cd doped IGZO	450 (B)	Non-volatile	8.0E-11	1	2	0.16 nJ	[S3]
	N doped ZnSnO	650 (R)	Non-volatile	2.0E-10	10.1	1	2.02 nJ	[S4]
		550 (G)	Non-volatile	2.3E-10			2.323 nJ	
		450 (B)	Non-volatile	8.0E-10			8.08 nJ	
	Undoped ZnSnO	635 (R)	Volatile	2.75E-11	1	10	10.4 pJ	This study
		519 (G)	Volatile	1.76E-12			17.6 pJ	
		454 (B)	Non-volatile	2.75E-11			275 pJ	
	Li doped Zanons	635 (R)	Non-volatile	2.04E-11	1	10	204 pJ	
		519 (G)	Non-volatile	4.35E-11			435 pJ	
		454 (B)	Non-volatile	1.29E-9			12.9 nJ	

[S1] C. Jo, J. Kim, J. Y. Kwak, S. M. Kwon, J. B. Park, J. Kim, G. S. Park, M. G. Kim, Y. H. Kim and S. K. Park, *Adv. Mater.*, 2022, **34**, 2108979.

[S2] R. Dutta, M. Naqi, Y. Cho, J. Oh, T. Kim, U. Jeong, Y. Yu, Y. Lee, S. Kim, *Adv. Funct. Mater.*, 2024, **34**, 2315058.

[S3] J. H. Jeong, M. H. Park, H. Jeong, W. Kim, S. Park, W. Jeon, S. J. Kang, *ACS Appl. Electron. Mater.*, 2023, **5**, 6275−6285.

[S4] X. Liu, J. Ren, P. Hu, Y. Qian, T. Li, L. Liang, H. Cao, *Phys. Status Solidi RRL*, 2024, **18**, 2300490.